JGR Atmospheres

RESEARCH ARTICLE
10.1029/2019JD030903

Special Section:
Bridging Weather and Climate: Subseasonal-to-Seasonal (S2S) Prediction

Impact of Snow Initialization in Subseasonal-to-Seasonal Winter Forecasts With the Norwegian Climate Prediction Model

F. Li[1], Y. J. Orsolini[1], N. Keenlyside[2], M.-L. Shen[2], F. Counillon[3], and Y. G. Wang[3]

[1]NILU – Norwegian Institute for Air Research, Kjeller, Norway, [2]Geophysical Institute, University of Bergen, Bergen, Norway, [3]Nansen Environmental and Remote Sensing Center, Bergen, Norway

Key Points:
- Eurasian snow strongly impacts surface temperature and upward wave activity flux
- High initial Eurasian snow favors the maintenance of the negative Arctic Oscillation though a land surface–stratosphere feedback
- Localized skill increments in surface temperature over the midlatitude snow transition regions even at lead times longer than 30 days

Correspondence to:
F. Li,
lifei-715@163.com

Citation:
Li, F., Orsolini, Y. J., Keenlyside, N., Shen, M.-L., Counillon, F., & Wang, Y. G. (2019). Impact of snow initialization in subseasonal-to-seasonal winter forecasts with the Norwegian Climate Prediction Model. *Journal of Geophysical Research: Atmospheres*, *124*, 10,033–10,048. https://doi.org/10.1029/2019JD030903

Received 29 APR 2019
Accepted 22 AUG 2019
Accepted article online 29 AUG 2019
Published online 18 SEP 2019

Abstract Snow initialization has been previously investigated as a potential source of predictability at the subseasonal-to-seasonal (S2S) timescale in winter and spring, through its local radiative, thermodynamical, and hydrological feedbacks. However, previous studies were conducted with low-top models over short periods only. Furthermore, the potential role of the land surface-stratosphere connection upon the S2S predictability had remained unclear. To this end, we have carried out twin 30-member ensembles of 2-month (November and December) retrospective forecasts over the period 1985–2016, with either realistic or degraded snow initialization. A high-top version of the Norwegian Climate Prediction Model is used, based on the Whole Atmosphere Community Climate Model, to insure improved coupling with the stratosphere. In a composite difference of high versus low initial Eurasian snow, the surface temperature is strongly impacted by the presence of snow, and wave activity fluxes into the stratosphere are enhanced at a 1-month lag, leading to a weakened polar vortex. Focusing further on 7 years characterized by a strongly negative phase of the Arctic Oscillation, we find a weak snow feedback contributing to the maintenance of the negative Arctic Oscillation. By comparing the twin forecasts, we extracted the predictive skill increment due to realistic snow initialization. The prediction of snow itself is greatly improved, and there is increased skill in surface temperature over snow-covered land in the first 10 days, and localized skill increments in the mid-latitude transition regions on the southern flanks of the snow-covered land areas, at lead times longer than 30 days.

1. Introduction

There is now a renewed concerted international effort to improve forecast skill at the subseasonal-to-seasonal timescale (S2S; defined here as the time range between 10 days to one season), which is nested between the timescale of weather forecasts and the timescale of seasonal prediction (Mariotti et al., 2018; Vitart & Robertson, 2018). The short-range weather forecasts largely depend on the accuracy of atmospheric initial conditions. As information contained in the initial atmospheric state is gradually lost (typically over 10 days), the actual predictability decreases. S2S prediction can be considered as extended-range weather forecasting, relying on both the atmospheric initial conditions and the more slowly evolving components of the climate system (Vitart et al., 2012; White et al., 2017).

Traditionally, coupled air-sea interactions at low latitudes, such as the El Niño–Southern Oscillation (ENSO) or the Madden-Julian Oscillation phenomena have been relied upon to provide enhanced seasonal or S2S prediction skill in the extratropics through their influence on Rossby wave propagation (Cassou, 2008; Smith Smith et al., 2016). Surface processes can also provide a source of S2S predictability. Soil moisture couples the land and the atmosphere, principally in the warm season, through changes in the evaporation and in the surface energy budget. Extensive multimodel studies consisting of multidecadal retrospective forecast experiments conducted during the Global Land–Atmosphere Coupling Experiment (GLACE2) project (Koster et al., 2010, 2011; van den Hurk et al., 2012) demonstrated how soil moisture initialization increases the predictive skill in near-surface (2 m) air temperature (TSAT) and, marginally, in precipitation at the S2S timescale, especially over the semiarid continental interiors, at the boundary of wet and dry climatic zones.

Besides soil moisture, snow is another surface variable that has received attention as a source of S2S predictability. The continental snowpacks over Eurasia or North America can influence the local surface

energy budget and TSAT, and the large-scale circulation patterns in winter (Dutra et al., 2011; Fletcher et al., 2009; Li & Wang, 2014; Orsolini & Kvamstø, 2009; Peings et al., 2012; Sobolowski et al., 2007) or in the spring (Broxton et al., 2017; Halder & Dirmeyer, 2016; Thomas et al., 2016; Xu & Dirmeyer, 2011). A thick snowpack tends to raise surface albedo and increases the soil moisture during snowmelt; its insulating property decouples the atmosphere from the warmer soil layers below. Hence, snow is involved in a combination of radiative, thermodynamical, and hydrological feedbacks at the surface. Regarding its influence on the large-scale circulation, the Eurasian autumn snow cover has been shown to alter the vertical propagation of Rossby waves into the stratosphere and thereby the stratospheric polar vortex, with a lagged surface impact projecting onto the Arctic Oscillation (AO), as a result of the downward propagation of zonal-mean anomalies induced by wave-mean flow interactions (e.g., Cohen et al., 2007, 2010, 2014; see Henderson et al., 2018, for a review). It is worthy to note, however, that many climate models fail to reproduce the apparent longer-lead linkage between autumn Eurasian snow cover and the winter-mean AO, inferred from observations (Furtado et al., 2015; Hardiman et al., 2008). Possible reasons could be the weak interannual variability in modeled snow cover, the lack of sensitivity to surface forcings, and the deficiencies in constructive interference between snow-induced and background planetary waves; this longer-lead linkage is also nonstationary (see Henderson et al., 2018, for a review of all these issues).

More specifically, the impact of snow initialization on S2S forecasts in the cold season was investigated in two studies that showed a moderate TSAT predictive skill improvement (Jeong et al., 2013; Orsolini et al., 2013). Following the aforementioned GLACE2 approach, these two studies, using either the fully coupled forecast model of the European Centre for Medium-range Weather Forecasts (ECMWF; Orsolini et al., 2013), or the Community Atmosphere Model (CAM; Jeong et al., 2013), examined forecast skill increments between twin experiments with either realistic or else degraded initial snow states. Firstly and foremost, realistic snow initialization increases the forecast skill of snow itself. Improving skill for snow in S2S and seasonal prediction systems is an important activity per se with many hydrological or cryospheric applications (He et al., 2016; Sospedra-Alfonso et al., 2016). In addition, significant forecast skill increments were found in TSAT over some regions of Eurasia and the Arctic in winter, up to a lead time of 1–2 months. The two aforementioned forecast studies suffered from several limitations. First, simulations were performed with low-top models; secondly, the S2S forecasts were evaluated over a short period only, for example, 6 years in Orsolini et al. (2013) and 12 years in Jeong et al. (2013). Thirdly, the areas with positive skill increments were not extensive. These skill increments partly resulted from local surface coupling between snow and TSAT, but improvement in modeled snow might also improve the large-scale circulation and thereby, indirectly, TSAT.

In addition, there could still be additional untapped forecast skill at the S2S timescale resulting from the snow-stratospheric teleconnection pathway. Orsolini et al. (2016) demonstrated that the Eurasian snow cover contributed to the persistence of the negative North Atlantic Oscillation (NAO) during the winter of 2009/2010, via such a stratospheric pathway. By making large changes in the snow initial states (yet within the bounds of the snow seasonal cycle) in the ECMWF forecast system, that study demonstrated that a thicker snow cover implied a colder surface, stronger meridional eddy heat fluxes up to the stratosphere, a weakened polar vortex, and a more persistent negative NAO as diagnosed in surface pressure. Hence, while snow was not the main driver of the NAO fluctuations, it contributed to its persistence at the S2S timescale.

In the present study, we evaluate the contribution of snow initialization to the S2S predictability over the northern hemisphere in winter, using a high-top version of the Norwegian Climate Prediction Model (NorCPM). To this end, we performed two sets of 2-month, ensemble, retrospective forecasts starting on 1 November over the period 1985 to 2016 with either realistic or degraded (via scrambling) initialization of the snow variables. We emphasize both the local and remote impacts of snow initialization on surface temperature and atmospheric circulation, and their potential impact on skill.

2. Model Experiments and Methodology

2.1. The Norwegian Climate Prediction Model High-Top Version

NorCPM is an initialized seasonal-to-decadal climate prediction system (Counillon et al., 2014, 2016) that combines the Norwegian Earth System Model (NorESM; Bentsen et al., 2013) and advanced data assimilation techniques based on the Ensemble Kalman Filter approach (Evensen, 2003). The ocean component is an

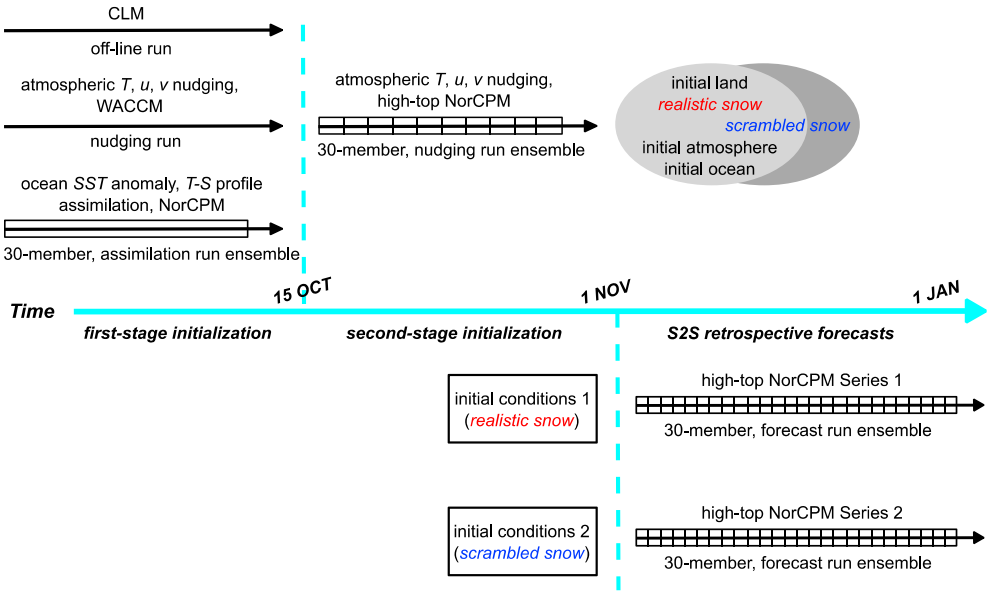

Figure 1. A schematic of the two sets of retrospective ensemble subseasonal-to-seasonal (S2S) prediction experiments with realistic and "scrambled" snow initial conditions in high-top Norwegian Climate Prediction Model (NorCPM).

updated version of the Miami Isopycnic Coordinate Ocean Model (MICOM; Bleck et al., 1992). In this study, we developed a high-top variant of NorCPM, in which the atmospheric component (normally the CAM model) is replaced with the Whole Atmosphere Community Climate Model (WACCM) version 4 (Marsh et al., 2013). WACCM extends vertically into the mesosphere-lower thermosphere region (up to 5.9×10^{-6} hPa, approximately 140 km). In addition, it incorporates an interactive stratospheric chemistry package and a parameterization of orographic and nonorographic (convective and frontal) gravity waves. In the present study, the atmosphere and land models have a horizontal resolution of 1.9° × 2.5° (termed f19, for the approximately 2° finite volume grid). The atmospheric model has 66 vertical levels. The ocean and sea-ice models have a horizontal resolution of 1° on a tripolar grid. The ocean model uses 53 isopycnal layers.

2.2. Initialization

Following the approach of GLACE2 (Koster et al., 2010) and SNOWGLACE (Orsolini et al., 2013), we perform twin ensembles of retrospective forecasts with either realistic or "scrambled" initial snow states. Starting from 1 November, the 2-month (November and December) retrospective forecasts are conducted from 1985 to 2016. The two ensembles of forecasts are nearly identical as they use the same realistic initial atmospheric and oceanic conditions, and their land initial conditions differ only wherever the snow is present on land (in either hemisphere).

More specifically, the initialization procedure (see Figure 1) is performed in two stages. The first stage ensures that the atmospheric model is realistically initialized using reanalysis data, and provides initial conditions for the second stage, where a coupled simulation intends to minimize initial shock. In the first stage,

1. The initial land state is taken from an off-line run of the Community Land Model (CLM version 4.5; Oleson et al., 2013), forced by boundary data from the Climatic Research Unit-National Center for Environmental Prediction (CRUNCEP) reanalyses.
2. The atmospheric state is initialized following a 14-day nudging period of WACCM to the ERA-Interim reanalyses (ERA-I; Dee et al., 2011), started from WACCM default atmosphere. The strong nudging includes three model prognostic variables (zonal and meridional winds and temperature) in the troposphere and in the stratosphere, but does not include the model diagnostic variables (humidity, cloud, etc.) in order to avoid increasing inconsistency due to imperfect subgrid parameterization (Karspeck et al., 2018).
3. The oceanic and sea-ice states are initialized from a NorCPM ensemble analysis, produced by assimilation of sea surface temperature (SST) and oceanic temperature and salinity profiles, which update the

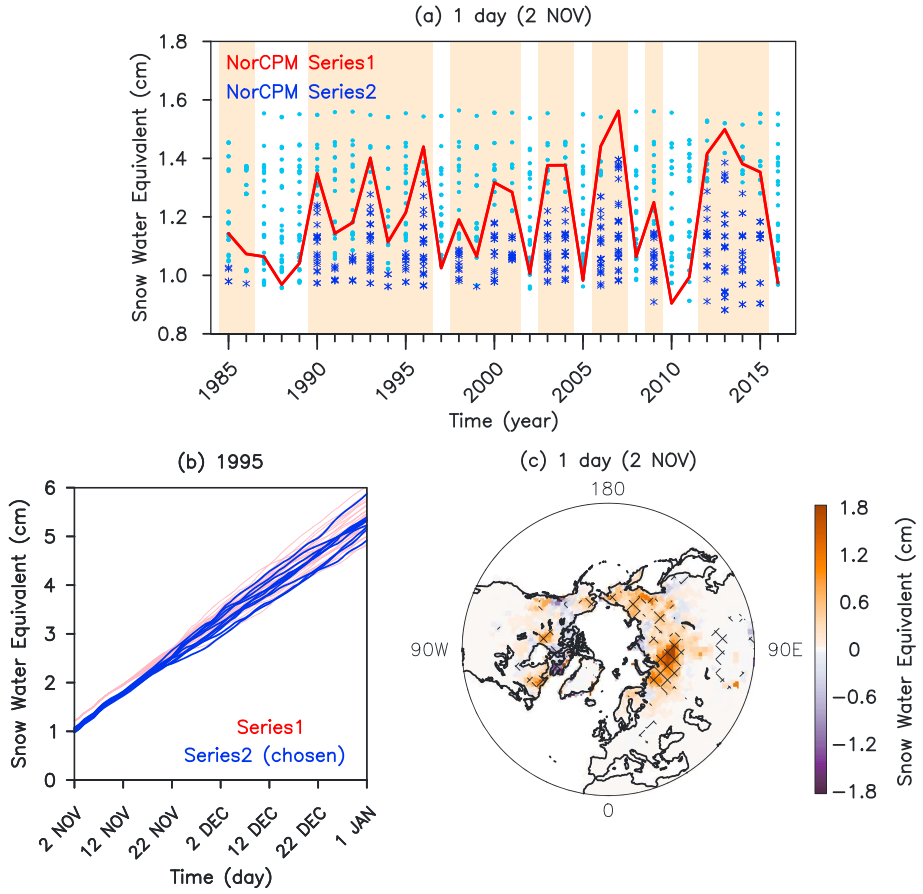

Figure 2. (a) Interannual variations of Eurasian snow water equivalent (SWE; cm) at day 1 (2 November; 1985–2016). Series 1: 30-member ensemble-mean (red curve); Series 2: members that have substantially lower (0.5 standard deviation for Series 1) Eurasian SWE than Series 1 (blue crosses) and other members (skyblue dots). (b) Example of time evolution of SWE through the forecast period, in the year 1995. All members of Series 1 (light pink), along with the members chosen for the conditional (i.e., lower) sampling of Series 2 (blue). (c) The initial difference of SWE between Series 1 and the conditional Series 2 at day 1 for the 22-year average (i.e., years with almond stripes in a). In Figure 2c (and in following Figures 4, 5, 6b, and 7), the 30-member ensemble-mean of Series 1 and the ensemble-mean of the conditionally sampled Series 2 (blue crosses, see text for explanation) are used. Crosses indicate regions where statistical significance exceeds the 95% confidence interval, based on a Monte Carlo test (here and hereafter).

ocean and the multicategory sea-ice model state. During the analysis, the atmospheric model is freely evolving but is responding to surface flux changes (e.g., over ocean). The assimilation uses observed, monthly anomalies in order to limit assimilation shock (Wang et al., 2017).

4. The 30 members of the ensemble forecasts start from the 30 different initial oceanic and sea-ice states in this ensemble analysis. Hence, the initial ensemble spread arises from the different oceanic and sea-ice conditions.

This first stage provides the initial conditions for the second-stage nudging, which is then performed over a 17-day period, but this time using the fully coupled NorCPM model to bring these different atmospheric, land, and ocean components into adjustment, prior to the forecasting stage. The atmospheric component of NorCPM is again nudged to ERA-I. In this second stage, each individual member of the ensemble is nudged until the forecast start date, in order to limit initial shocks.

In the first ensemble (hereafter Series 1 following the GLACE2 nomenclature), the snow variables are realistically initialized and are identical for all members. In the second set (hereafter Series 2), the snow variables are scrambled, taken at random from the remaining years (but still pertaining to November 1). Each ensemble member in Series 2 has a different randomized, initial snow state, in which the 13 prognostic snow variables listed in Table 1 are scrambled in a consistent manner. While individual members of Series 2 can

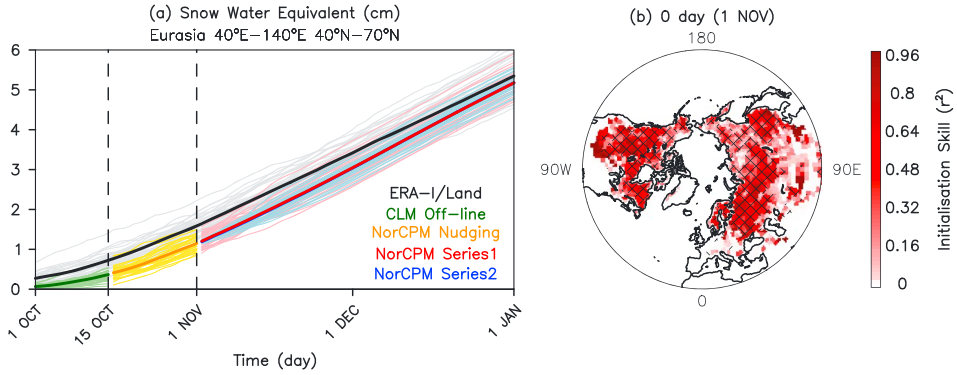

Figure 3. (a) Daily evolution of Eurasian (40–140°E, 40–70°N) snow water equivalent (SWE; cm) in ERA-I/La nd (1 October–1 January; black-gray), Community Land Model (CLM) off-line run (1–15 October; green), ensemble-mean Norwegian Climate Prediction Model (NorCPM) nudging run (16 October to 1 November; orange-yellow), and NorCPM Series 1 (red) and Series 2 (blue) ensemble-mean forecasts (2 November-1 January). The thin lines indicate ensemble-mean SWE for 32 years (1985–2016) individually, and the thick lines are the 32-year averages. The spread of the ensemble means for Series 1 is representative of interannual variability (thin red lines); in contrast, the ensemble means for Series 2 are initially nearly identical from year to year (thin blue lines) and are approximately equal to the 32-year average of Series 1 (thick blue line, nearly identical to thick red line). (b) The initialization skill (r^2, with the sign of r) of SWE on 1 November between ensemble-mean NorCPM nudging run and ERA-I/Land.

have either less or more snow than prescribed in Series 1 at the initial time (1 November), the climatological ensemble-mean initial difference between Series 1 and 2 is very small.

2.3. Diagnostics

Series 1 and 2 each consists of 960 simulations (32 winters × 30 members), providing a large enough sample to test the impact of snow initialization on predictability. The forecasted atmospheric variables are evaluated against ERA-I reanalyses, and the forecasted snow against ERA-I/Land reanalyses (a version without precipitation correction, here referred to as an uncorrected version; Balsamo et al., 2015). The forecast skill for each series is quantified by the r-square metric (r^2). Here, r indicates anomaly correlation coefficient obtained by verifying ensemble-mean forecasts against reanalyses. The reanalysis anomaly is calculated from the 1985–2016 climatology. The forecast anomaly is the departure from the 30-member climatology over the same period. When taking the difference in r^2 between Series 1 and 2, we have multiplied each r^2 by the sign of r, following van den Hurk et al. (2012) to avoid rewarding degradation in Series 2. A positive r^2 difference between Series 1 and 2 indicates a location where the difference in snow initialization improved the skill, supposing that the statistical noise is negligible. The statistical significance is assessed using a Monte-Carlo approach based on 1,000 random reshufflings of the observational anomalies. The diagnostics were averaged in 10-day subperiods, six per forecast, corresponding to lead times of 0 (days 1–10), 10 (days 11–20), 20 (days 21–30), 30 (days 31–40), 40 (days 41–50), and 50 (days 51–60) days, respectively. Prior to analyses, the reanalysis data are regridded to the model horizontal grid (1.9° longitude × 2.5° latitude).

Our diagnostic approach is twofold. We want to determine possible skill improvement in Series 1 compared to Series 2 using the entire forecast ensembles (section 3.4). We also want to explore the mechanisms by which snow may impact TSAT and the atmospheric circulation (sections 3.2 and 3.3) and, to this end, it is useful to make a composite difference between high and low initial snow states. Our primary focus is the Eurasian snow cover and we now explain how we construct this high minus low Eurasian snow composite difference. Figure 2a shows the spread and interannual variability of the initial snow states, namely, the Eurasian snow water equivalent (SWE) at day 1 (2 November) for Series 1 (for the 30-member ensemble-mean in red, noting that all members in Series 1 have nearly identical SWE at day 0), and for the 30 individual members of Series 2 (blue crosses and skyblue dots, the use of two different symbols to be explained below). We reiterate that since the snow variables in Series 2 were scrambled at day 0 from the 1 November snow states in other years, the spread of the 30 members in Series 2 is representative of interannual variability. Next, we construct a composite difference using a conditional sampling of Series 2: that is, by taking the difference between the Series 1 ensemble-mean and a Series 2 ensemble-mean that retains only the members of Series 2 that have less initial Eurasian SWE than Series 1, in any particular year. We

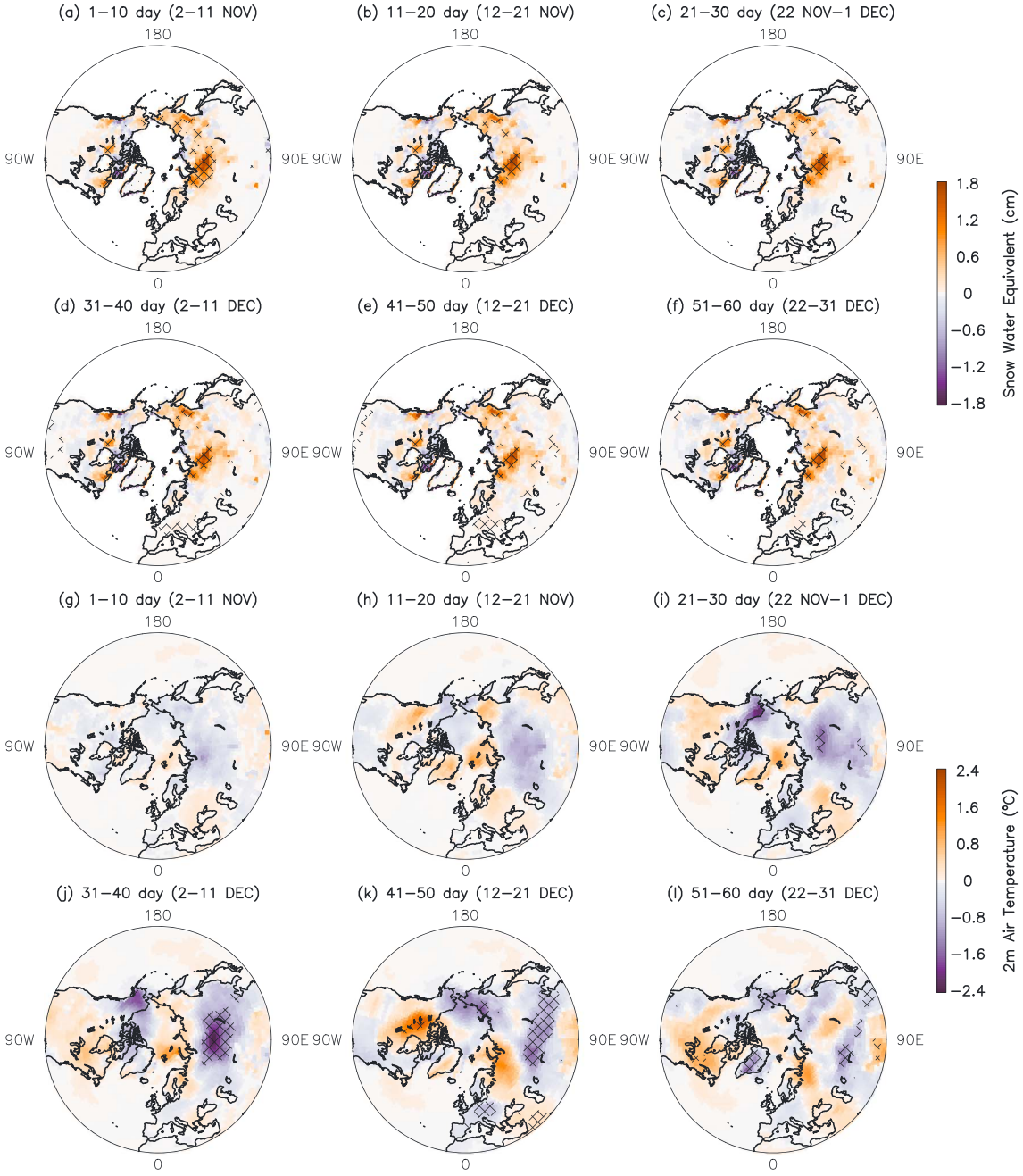

Figure 4. The differences of (a–f) snow water equivalent (cm) and (g–l) 2-m air temperature (TSAT; °C) between Series 1 and the conditionally sampled Series 2 for the 22-year average, as a function of lead time (ranging from 0- to 50-day lead times).

further require that the snow difference is large enough, below −0.5 standard deviation (see Figure 2b), so that the composite difference reflects substantially different initial snow states. The members of Series 2 retained (i.e., with low initial SWE and obeying the aforementioned criterion) are indicated by blue crosses in Figure 2a. Following that procedure, there are some years when the conditionally sampled Series 2 has no member, and we neglect these years to retain only the 22 years with at least one member (in Figure 2a, the selected years are indicated by almond stripes). Figure 2c illustrates the initial SWE difference (Series 1 minus the conditionally sampled Series 2) at day 1 for the 22-year average, which we take as equivalent to a snow composite difference (high minus low Eurasian snow). Higher SWEs are found indeed over most of Siberia with a maximum over 1.5 cm, to the east to the Ural Mountains. Note that the

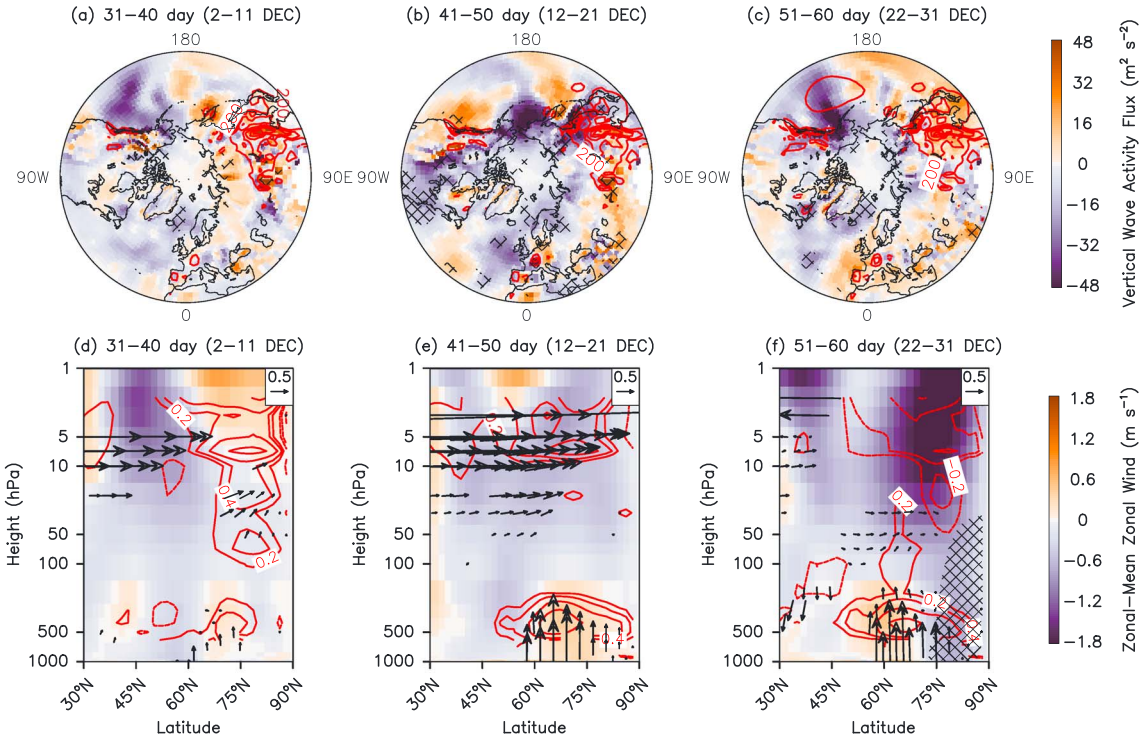

Figure 5. The differences of (a–c) 500-hPa vertical wave activity flux (shaded; $m^2 \cdot s^{-2}$; Plumb, 1985) and (d–f) zonally-averaged zonal wind (shaded; $m \cdot s^{-1}$), Eliassen-Palm (E-P) flux cross sections (vectors; $m^2 \cdot s^{-2}$) and its divergence (red contours; $m \cdot s^{-1} \cdot day^{-1}$) between Series 1 and the conditionally sampled Series 2 for the 22-year average, at (a and d) 30-day, (b and e) 40-day, and (c and f) 50-day lead times. The red contours in (a–c) indicate the 22-year climatology of Series 1. To display the E-P flux throughout the stratosphere, vectors are scaled by $\sqrt{1,000/p}$ and the inverse of the air density. Additionally, the vertical component is multiplied by 125.

snow evolution in given members of Series 2 in given years may be such that it does not remain lower than Series 1 throughout the length of the forecast, albeit it was at the initial time (see Figure 2b for example).

3. Results

3.1. Initialized SWE

In order to illustrate the snow evolution during the two nudging initialization stages as well as during the forecasts, Figure 3a shows the daily time series of SWE averaged over Eurasia (40–140°E, 40–70°N) from 1 October to 1 January, for the climatological mean (1985–2016, thick lines) and for each individual year (thin lines). The snow evolution is hence shown during the CLM off-line run (green lines), the full NorCPM nudging stage (yellow lines with orange 32-year mean), and during the Series 1 (red lines) and Series 2 (blue lines) forecasts. For reference, we also plotted the snow from ERA-I/Land reanalyses (grey lines with black 32-year mean). There is a climatological bias in the modeled SWE compared to ERA-I/Land, which amounts to −0.43 cm on 1 November. Figure 3b shows the skill (r^2) of the initial snow states (in terms of in SWE) against ERA-I/Land on 1 November. The skill is largely positive at high latitudes and is as high as 0.8 over Russia, the Far East, and North America, indicating that the interannual variability of snow initial states produced by our initialization method is representative of realistic conditions.

3.2. Differences in Snow and Surface Temperature Between Series 1 and the Conditionally Sampled Series 2

The focus of this section is to examine the local thermodynamic feedback and the hemispheric-scale dynamical interactions between the snow and the atmosphere. The surface impact of the high versus low snow initial conditions over Eurasia is revealed in Figure 4 in terms of SWE and TSAT in the 22-year composite difference between Series 1 and the conditionally sampled Series 2, as defined in the previous section. The results are presented as a function of lead time and valid for 10-day periods (ranging from 0- to 50-day

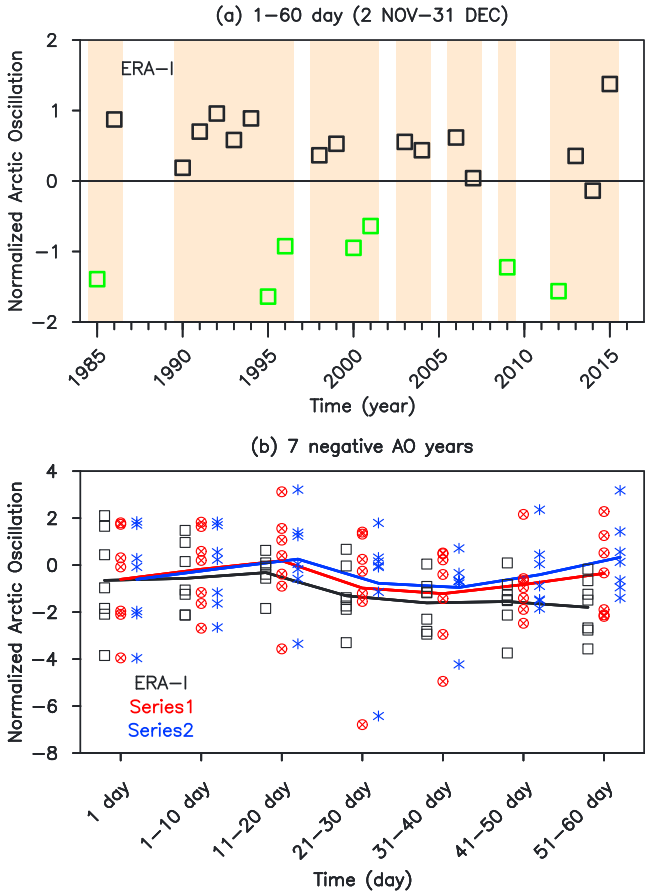

Figure 6. (a) Interannual variations of the normalized Arctic Oscillation (AO) index in early winter (days 1–60) in ERA-Interim for the 22 years used in the composite analysis (indicated by almond stripes). The green squares indicate the 7 negative AO years. (b) Evolution of the normalized AO indices during each 10-day subperiod in ERA-Interim (black squares), throughout the Series 1 ensemble-mean forecasts (red circles with cross), and the conditionally sampled Series 2 forecasts (blue crosses). The value at day 1 is also indicated to reflect initial conditions. Markers indicate ensemble-mean AO indices for 7 negative AO years individually, and lines are the 7-year averages.

lead times). Series 1 has higher SWEs initially over Siberia (by the composite design), and these are maintained throughout the entire early winter (Figures 4a–4f). At the 0- and 10-day lead times, Series 1 exhibits the expected local surface cooling in response to the positive Siberian snow anomaly (Figures 4g and 4h). Interestingly, the TSAT response at longer lead times (20-day and beyond) migrates southward toward Eurasian mid-latitudes (where the snow edge line is located) and is statistically significant at the 95% level there (Figures 4i–4l).

Figures 5a–5c illustrate the composite differences in the 500-hPa vertical wave activity flux at the 30-, 40-, and 50-day lead times, along with its climatology, while Figures 5d–5f illustrate the corresponding height-latitude cross sections of zonal-mean Eliassen-Palm (E-P) flux(i.e., zonal average of wave activity flux) and its divergence, along with the zonal-mean zonal wind. Starting more prominently at the 40-day lead time, the upward wave activity over Siberia increases (positive anomalies in Figures 5b–5c). Meanwhile, the E-P flux vectors bend more upward in the troposphere and poleward in the stratosphere (vertical and horizontal arrows in Figures 5e–5f). Because an upward (equatorward) pointing E-P flux vector is proportional to poleward eddy heat flux (poleward meridional eddy momentum flux), the poleward E-P flux vectors in the stratosphere and the upward E-P flux vectors in the troposphere (Figures 5e–5f) indicate that (1) there is a deceleration of the zonal-mean zonal wind at high latitudes (Figure 5f), and (2) the polar vortex is coherently weaker throughout the stratosphere, although the difference is only significant in the lower stratosphere. Arguably, these high versus low snow composite differences indicate that due to the positive snow forcing and associated cooler TSAT (Figure 4), there is enhanced wave flux into the stratosphere and a weakened polar vortex (Figure 5). Henderson et al. (2018) reviewed the proposed mechanisms by which an increased snowpack over Siberia in fall or early winter could be followed by a weakened polar vortex, and at least some studies—but not all—support such a linkage, as discussed in section 1. In our simulations, the stratospheric changes do not occur before the 30-day lead time, likely due to the surface temperature anomalies being larger at that time (Figure 4j) than at the initial time.

3.3. Snow/Stratosphere/AO Coupling During Negative AO Years

Further clues as to the role of snow emerge by looking specifically at the winters when the AO is markedly negative, since the feedback from the thicker and more extensive Siberian snowpack may then act to maintain the negative phase through surface–stratosphere coupling (Orsolini et al., 2016). For this purpose, a simple AO index is defined here as a sea level pressure (SLP) difference between the two latitude zones (35 and 65°N), and the normalized value of the zonal average is then subtracted (Li & Wang, 2003). In the 22 years considered in the compositing, there are 7 strongly negative AO years (Figure 6a: green squares), and we average the composite differences between Series 1 and the conditionally sampled Series 2 over these 7 years. Figure 7 shows this negative AO average in SLP, 300-hPa zonal wind, 150-hPa geopotential height, and 500-hPa vertical wave activity flux, at the 50-day lead time. The motivation for choosing this lead time will be best seen latter in Figure 6 b. Series 1 shows a more negative AO pattern in SLP (Figure 7a), a southward-displaced Atlantic westerly jet stream (Figure 7b), and an averaged positive 150-hPa geopotential anomaly over the polar cap (Figure 7c). These features in the composite difference are characteristics of a more pronounced negative AO. This is also supported by the enhanced wave activity flux at 500 hPa over Eurasia and eastern North Pacific (Figure 7d). Figure 6b further indicates that the AO index is indeed persistently more negative in Series 1 than in the conditionally sampled Series 2 since the 20-day lead time, when the observed AO becomes more negative. One may note the observed AO is much more negative and persistent than the

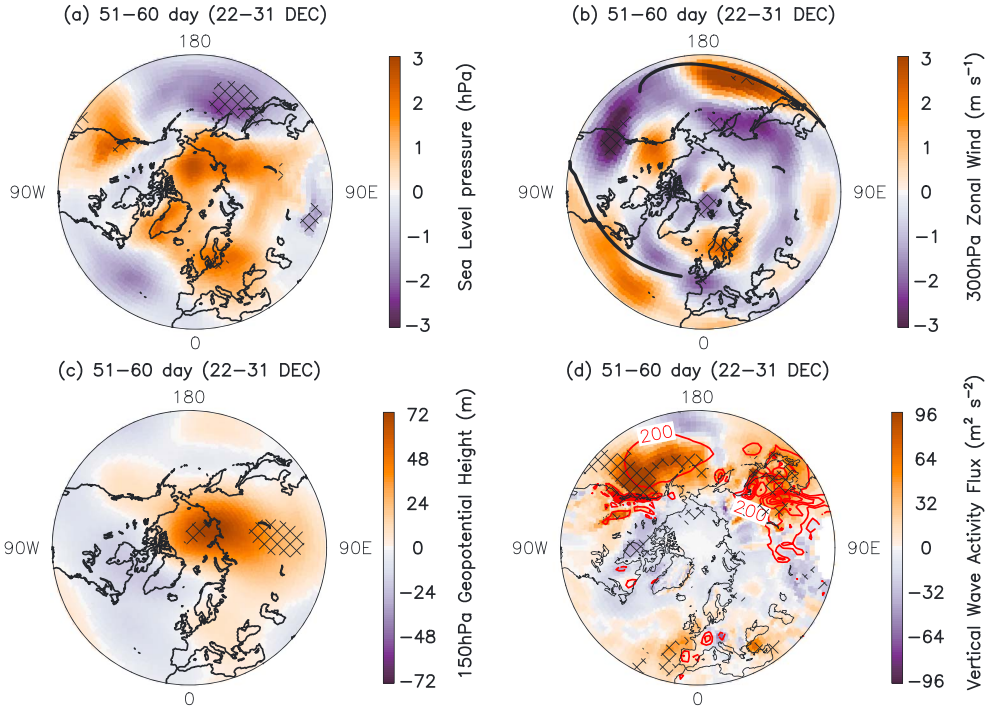

Figure 7. The differences of (a) sea level pressure (hPa), (b) 300-hPa zonal wind ($m \cdot s^{-1}$), (c) 150-hPa geopotential height (m), and (d) 500-hPa vertical wave activity flux (shaded; $m^2 \cdot s^{-2}$) between Series 1 and the conditionally sampled Series 2 for the average of 7 negative AO years, at the 50-day lead time. The black line in (b) indicates the axis of the climatological westerly jet stream for Series 1. The red contours in (d) indicates the 7-year climatology of Series 1.

forecasted values. As in Orsolini et al. (2016), our main point is not that the snow drives the AO fluctuations, but rather that it exerts a weak feedback that contributes to its persistence. The seemingly small amplitudes of the differences in the AO index, for example, 0.5 at 40-day lead, crucially depends on what is compared with Series 1. The snow perturbations imposed in Series 2 initial conditions were indeed small, characteristics of interannual variations, and not as large as the ones used in the 2009/2010 case study in Orsolini et al. (2016), characteristics of intraseasonal variations (their Figure 1).

3.4. Forecast Skill Increment Between Series 1 and 2

By using realistic oceanic, atmospheric, and land initial states, the NorCPM prediction system incorporates the potential sources of skill from SST, land, and atmospheric conditions altogether. We now further estimate the specific contribution of snow initialization to the predictability. Starting with SWE, Figure 8 illustrates the forecast skill (r^2) in Series 1 and the forecast skill difference (Series 1 minus Series 2) over the 32 years, as a function of lead time. As expected from the SWE initialization skill (Figure 3b), Series 1 tends to exhibit significant positive skill over most of the high latitudes (poleward of 45°N), which progressively decreases with time through the six subperiods (Figures 8a–8f). There is a notable large and coherent positive skill increment over both northern Eurasia and North America (Figures 8g–8l) up to the 50-day lead time. This demonstrates that the realistic snow initialization improves the forecast of snow itself throughout the 2-month forecast period, consistent with previous studies.

Turning to TSAT (Figures 9a–9f), the skill of Series 1 is close to 1 over both land and oceans at the 0-day lead time, indicating that the good quality of the initialization method, while generally decaying afterward, as expected from forecast degradation at the medium-range timescale. Over large

Table 1
The Snow Variables Scrambled in Series 2

Name	Long-name	Units
SNLSNO	number of snow layers	unitless
SNOWDP	snow depth	m
frac_sno	fraction of ground covered by snow	0 to 1
DZSNO	snow layer thickness	m
ZSNO	snow layer depth	m
ZISNO	snow interface depth	m
H2OSNO	snow water	mm
H2OSOI_LIQ	liquid water (only in the snow layer)	$kg \cdot m^{-2}$
H2OSOI_ICE	ice lens (only in the snow layer)	$kg \cdot m^{-2}$
T_SOISNO	soil-snow temperature	K
snw_rds	snow layer effective radius	um
albsnd_hst	snow albedo (direct)	0 to 1
albsni_hst	snow albedo (diffuse)	0 to 1

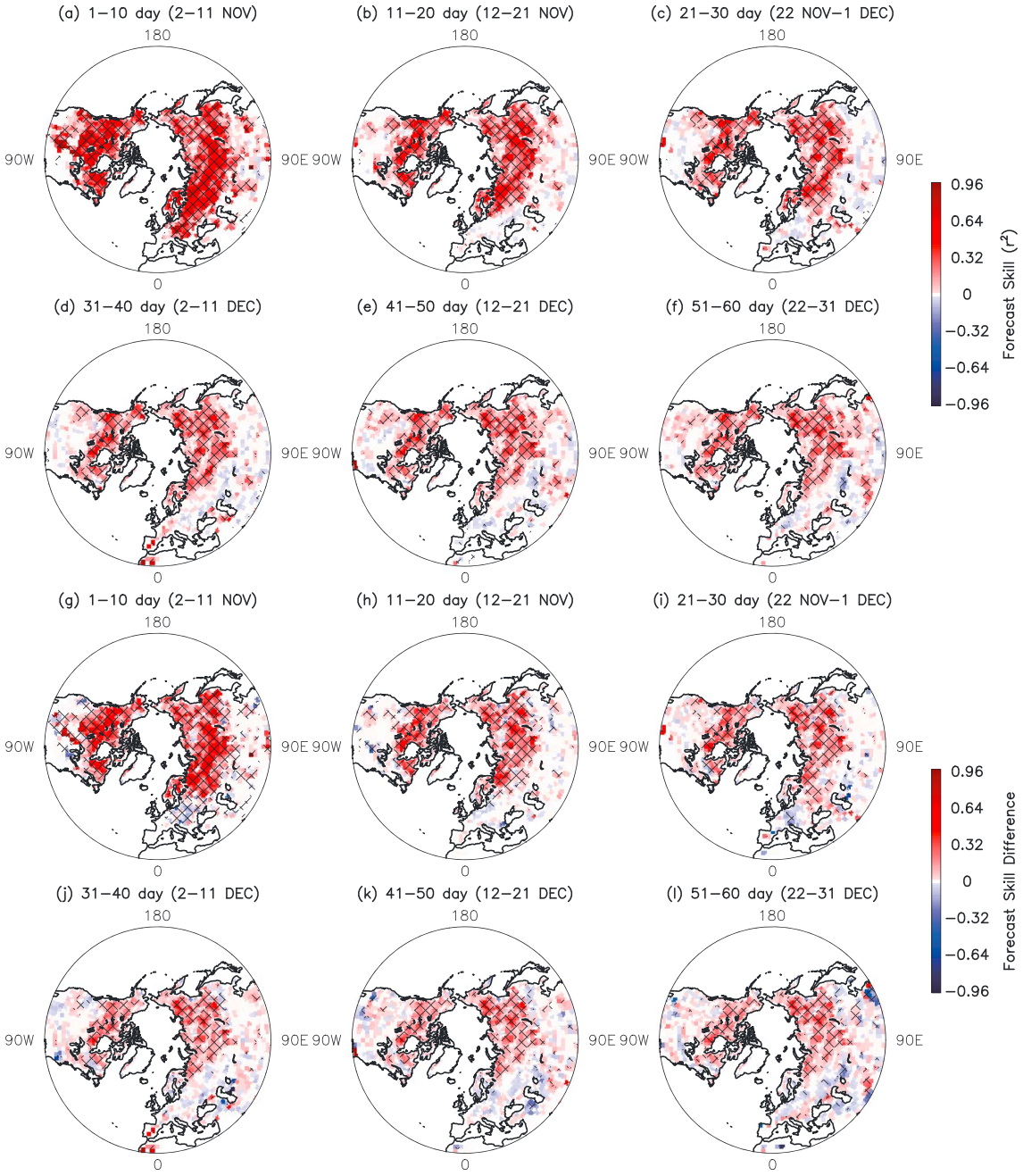

Figure 8. (a–f) The forecast skill (r^2) of snow water equivalent (SWE) for Series 1 and (g–l) the forecast skill differences of SWE between Series 1 and 2, as a function of lead time (ranging from 0- to 50-day lead times).

oceanic areas (i.e., parts of the North Pacific and Arctic Ocean), the skill persists up to the 50-day lead time while it rapidly decays after 20 days over the continents, indicating that this local skill persistence over the oceans arises from SSTs. The TSAT skill increment resulting from realistic snow initialization (Figures 9g–9i) is large over snow-covered land at the 0-day lead time (Figure 9g), indicating local feedback from the improved snow state, but it rapidly decays during the next lead time (Figure 9h).

Interestingly, at longer lead times, especially at the 30-day but also at the next lead times, there are localized positive skill increments. Hence, there is skill resurgence 1 month into the forecast. The maximum skill increments (up to 0.3–0.4) are of the same order as those obtained for soil moisture (Koster et al., 2010) or for snow in Thomas et al. (2016). The ratios of points north of 30°N with significant and positive skill

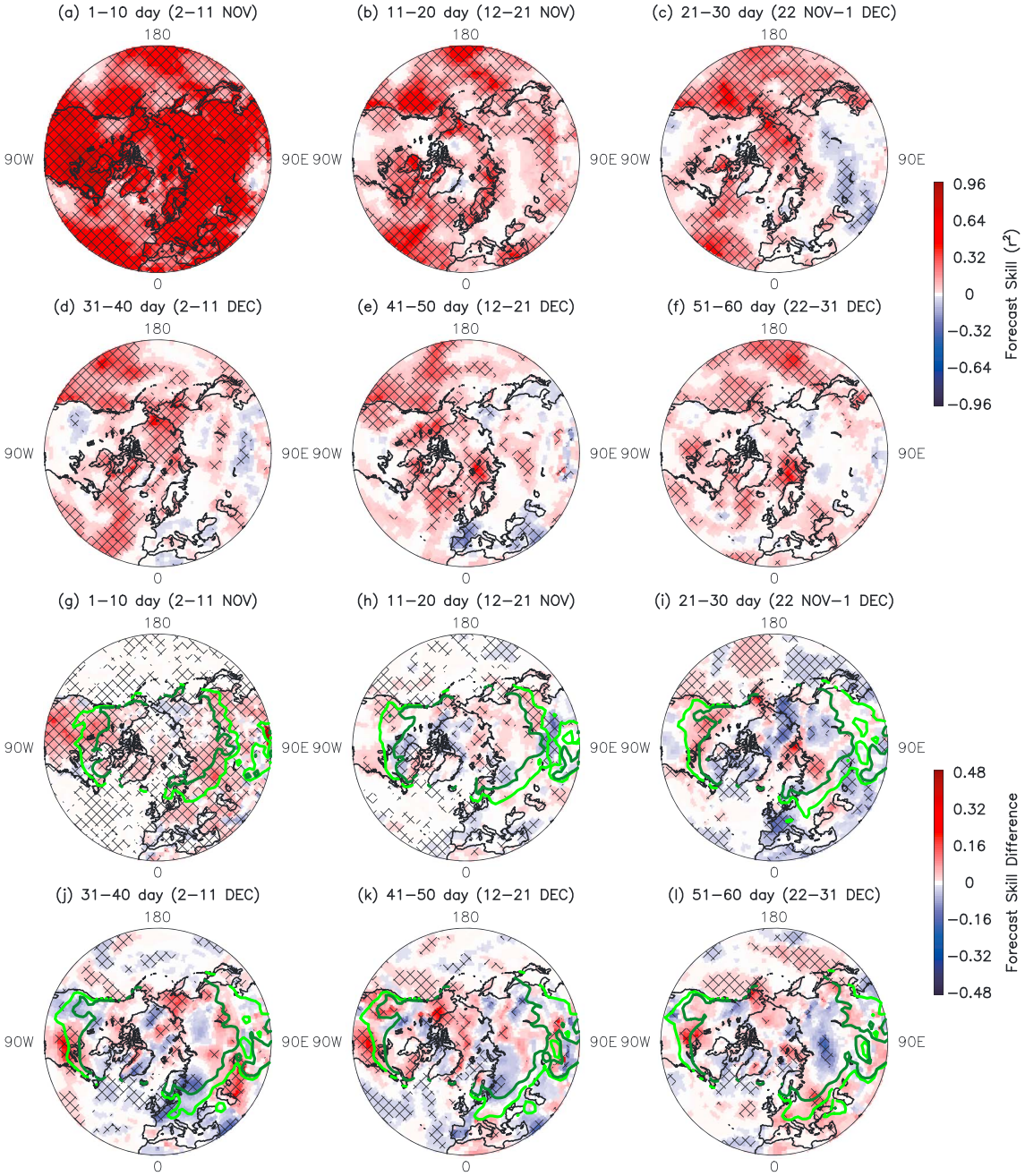

Figure 9. As in Figure 8 except for near-surface air temperature. The green and dark green contours in (g–l) indicate the mid-latitude snow transition regions, calculated as the 0.1 and 1 cm of the climatological snow water equivalent for Series 1.

differences to those with significant and negative differences are 3.70, 1.00, 0.67, 1.20, 2.18, and 1.64 at the 0-, 10-, 20-, 30-, 40-, and 50-day lead times, respectively. Hence, at the 40-day lead time, for example, there are twice more points with positive increments. These increments, albeit undoubtedly patchy, are situated in the transition regions between high and low snow on the southern flank of the snow-covered land areas, over parts of the Eurasian and North American continents at midlatitudes (Figures 9j–9l). The green and dark green contours in Figures 9g–9l delineate these climatological transition regions of low SWE.

The local coupling between snow and TSAT in these transition regions is supported by Figure 10, which shows the correlation-square (r^2, with the sign of r) between TSAT and SWE for Series 1as a function of lead time. Broad belts of negative correlations, associating cold and high snow anomalies, stretch across the

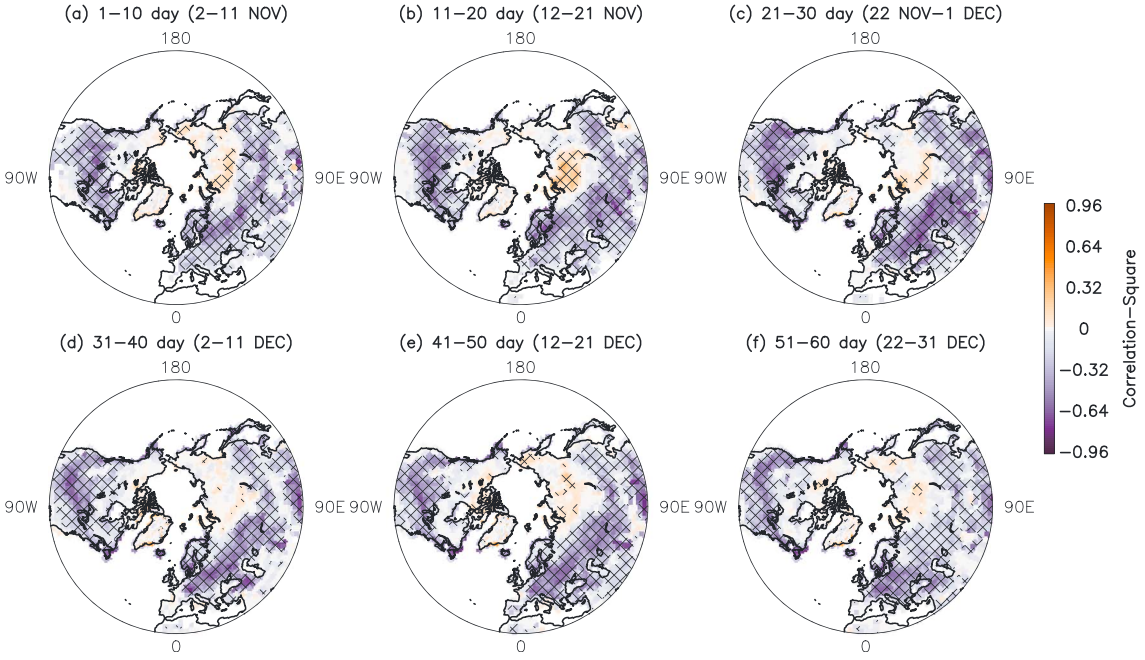

Figure 10. The correlation-square (r^2, with the sign of r) between near-surface air temperature and snow water equivalent for Series 1, as a function of lead time (ranging from 0- to 50-day lead times).

continents at midlatitudes, migrating southward as the winter season progresses. These broad continental belts correspond to the transition regions where TSAT predictability is sensitive to snow, while, at higher latitudes, SWE is always large and decouples from TSAT (Dutra et al., 2011; Thomas et al., 2016). In their study about soil moisture influence during the warm season, Koster et al. (2004) termed such transition regions "hot spots" of land-atmosphere coupling. Examining snow-atmosphere coupling in the spring in a potential predictability framework, Xu and Dirmeyer (2011, 2013) appropriately termed these regions "cold spots." As pointed out in the latter, the constraint of snow in Series 1 (where all the members have the same snow state initially) reduces the inter-member variance in TSAT compared to Series 2 (where the members have all different snow states, initially). This reduction in intermember variance or spread at the 0-lead time is shown in Figure 11, averaged over the 32 years.

3.5. Relation Between the Stratospheric Polar Vortex and Surface Conditions

We have demonstrated that modeled TSAT over Eurasia is strongly influenced by the presence of snow (Figure 4). However, there are other factors influencing the temperature. In particular, Garfinkel et al. (2017) demonstrated a relationship between the winter-mean (December–February) state of the stratospheric polar vortex and TSAT over Eurasia at the interannual timescale, associating cold Eurasian winter temperature to a weak polar vortex. In Figure 12, we verify if such an interannual covariability between the stratospheric polar vortex and Eurasian TSAT anomalies is captured in the NorCPM S2S ensemble-mean forecasts in November and December. We diagnose the lower stratospheric polar vortex strength in terms of the polar cap-averaged (poleward of 70°N) geopotential height at 150 hPa, while the Eurasian TSAT is averaged over the area (40–140°E, 40–70°N). There is indeed a significant correlation between the vortex strength and Eurasian TSAT in reanalysis data, with a correlation coefficient of −0.39 in November and −0.45 in December (statistical significance at the 95% and 99% confidence intervals, respectively), albeit weaker than the winter-mean correlation of −0.72 over a slightly different multidecadal period in

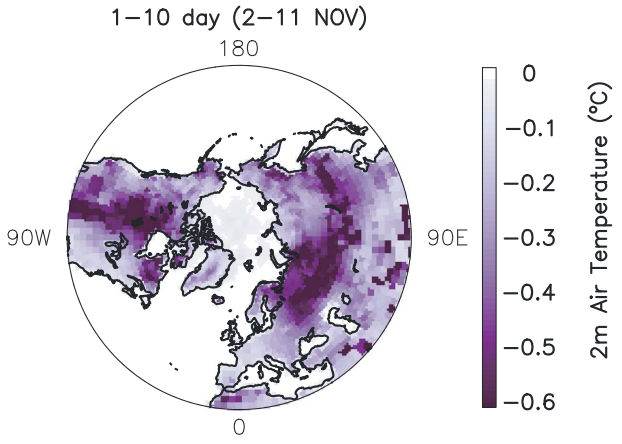

Figure 11. The differences of intra-member spread of near-surface air temperature (°C) between Series 1 and 2 for the 32-year average, at the 0-day lead time.

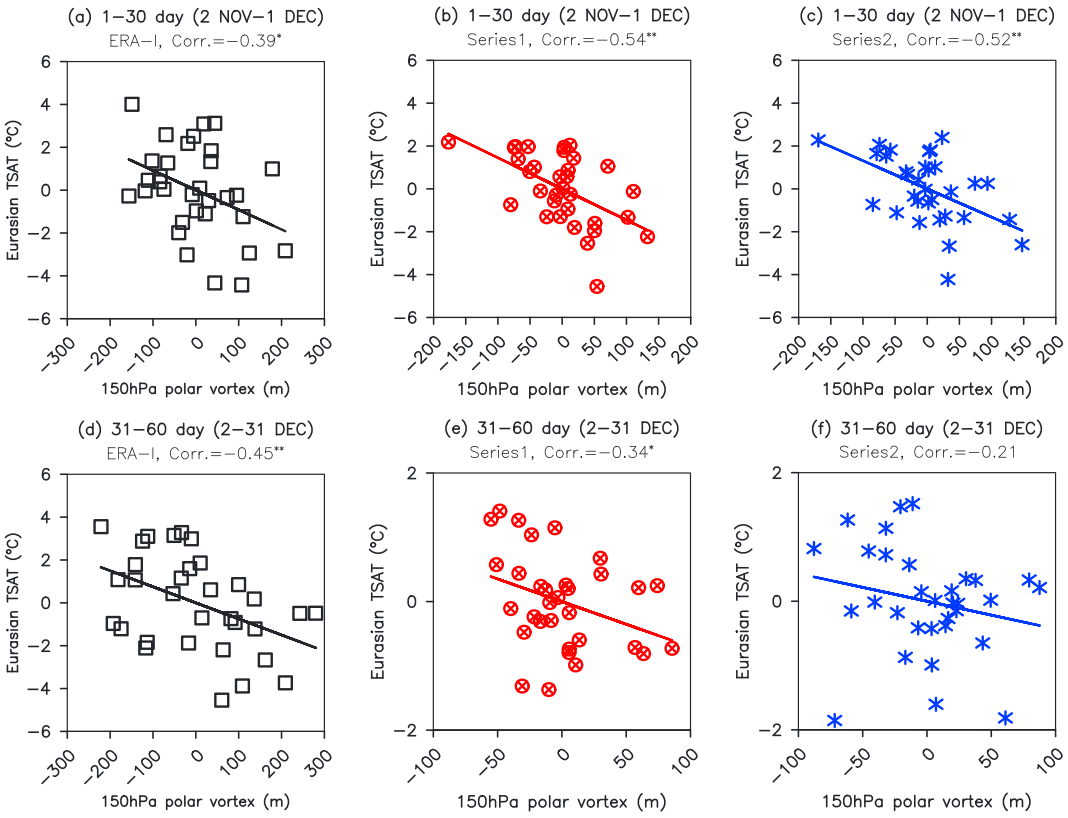

Figure 12. Scatter plots for TSAT (°C) over Eurasia (40–140°E, 40–70°N) and 150-hPa geopotential height (m) over the polar cap (poleward of 70°N) (a–c) in November (days 1–30) and (d–f) in December (days 31–60). Values are for (a and d) ERA-Interim, (b and e) Series 1, and (c and f) Series 2 ensemble-mean forecasts. Note the different scale for TSAT among the graphs.

Garfinkel et al. (2017). This relation is, to a large extent, captured in Series 1 with a correlation coefficient of −0.54 in November and −0.34 in December. The model internal dynamics coupling the stratosphere and the troposphere insures that this relation is captured in Series 2 as well. Since we are using here the full ensemble for Series 2, with members having either initial snow higher or lower than in Series 1, the differences with Series 1 are not large.

4. Summary, Discussion, and Outlook

Here, we have extended the studies of Orsolini et al. (2013, 2016) and Jeong et al. (2013) on the influence of snow initialization upon S2S forecasts by using a high-top model and a greatly increased analysis period covering 32 winters (1985–2016) and a larger ensemble size (30 members). By comparing twin 30-member ensembles of 2-month retrospective forecasts with accurate and degraded snow initialization, we extracted the additional predictive skill (or skill increment) due to a change in snow initialization representative of interannual variations. We see that (i) the prediction of snow itself is greatly improved by using the realistic initialization; (ii) there is, in the latter case, increased TSAT skill over snow-covered land at the 0-day lead time; and (iii) although the TSAT skill is low beyond 20 days, limited skill increments in the transition regions on the southern flank of the snow-covered land areas, at lead times longer than 30 days. The skill increments could result from local snow-atmosphere coupling or from improvements in the atmospheric circulation.

The actual values of the skill increments crucially depend on how much Series 2 were degraded by design, and are thereby somewhat artificial. Here, the snow perturbations used in Series 2 are fairly small, representative of interannual variations (see Figure 3a). More important is the location of the skill increase, suggestive of "cold spots" of local coupling between snow and TSAT in the mid-latitude snow transition regions (Dutra et al., 2011; Xu & Dirmeyer, 2011, 2013).

Using a composite difference of high versus low initial Eurasian snow constructed from a restricted (conditionally sampled) ensemble of Series 2 members, we also found that the TSAT response at longer lead times (20-day and beyond) migrates southward toward Eurasian midlatitudes, where the snow edge is located. Associated to the colder TSAT (Figure 4), there is enhanced wave flux into the stratosphere and a weakened polar vortex at 30- to 50-day lead times (Figure 5). Focusing further on 7 strongly negative AO years, we find that the AO index is indeed persistently more negative in Series 1 than in the conditionally sampled Series 2 after the first month, albeit not as negative and persistent as in the reanalyses (Figure 7). As in Orsolini et al. (2016), our main point is not that the snow drives the AO fluctuations, but rather that it exerts a weak feedback that contributes to its persistence.

Our snow initialization relies upon an off-line run of the CLM model (e.g., without snow data assimilation), which is then adjusted in the nudging stages. Hence, it relies on model-generated data, and this state of affairs still exists in several *operational* prediction systems (e.g., Jeong et al., 2017; Thomas et al., 2016), due to the poor spatial and temporal coverage of the observed snow depth data (or equivalently, SWE) needed to initialize land models. An initialization relying more on land data assimilation would be desirable. Heterogeneity of the land surface introduces model errors; this first version of NorCPM has a coarse atmospheric resolution (1.9° × 2.5°), a standard resolution for WACCM, but a higher resolution version would be desirable. Another important aspect in estimating actual skill for snow is the verification data. Here we verified the forecasted snow against ERA-I/land SWE, which is also produced by an off-line run of the ECMWF land model and has biases compared to CLM (see Figure 3a). Incidentally, the model SWE interannual variability is slightly underestimated compared to ERA-I/land, which may diminish the magnitude of the snow-atmosphere coupling. Newer, blended SWE products have been developed using an ensemble of gridded observational, satellite or in situ, products, and reanalyses, aimed at providing a mean SWE reference, a measure of observational uncertainty, and an estimation of regional or temporal biases in particular datasets (Mudryk et al., 2015). In the future, it would be of interest to test the snow prediction against such verification data to develop hydrological and cryospheric applications of the multidecadal S2S reforecasts.

Acknowledgments
We acknowledge ECMWF for making the SWE and atmospheric reanalysis data available. The ERA-I and ERA-I/Land products are available at ECMWF web interface. Retrospective forecast data are available on the Norwegian storage facility (NIRD, https://archive.sigma2.no/pages/public/datasetDetail.jsf?id=10.11582/2019.00014 with doi:10.11582/2019.00014). This study was supported by the Research Council of Norway (grants EPOCASA 229774/E10 and SNOWGLACE 244166) and the National Natural Science Foundation of China (grant 41605059). This work has received a grant for computer time (project number nn9385k and nn9039k), as well as storage space (project number ns9207k and ns 9039k) from the Norwegian e-infrastructure for Research & Education (Sigma2).

References

Balsamo, G., Albergel, C., Beljaars, A., Boussetta, S., Brun, E., Cloke, H., et al. (2015). ERA-Interim/Land: A global land surface reanalysis dataset. *Hydrology and Earth System Sciences*, *19*(1), 389–407. https://doi.org/10.5194/hess-19-389-2015

Bentsen, M., Bethke, I., Debernard, J. B., Iversen, T., Kirkevåg, A., Seland, Ø., et al. (2013). The Norwegian Earth System Model, NorESM1—Part 1: Description and basic evaluation of the physical climate. *Geoscientific Model Development*, *6*(3), 687–720. https://doi.org/10.5194/gmd-6-687-2013

Bleck, R., Rooth, C., Hu, D., & Smith, L. T. (1992). Salinity-driven thermocline transients in a wind- and thermohaline-forced isopycnic coordinate model of the North Atlantic. *Journal of Physical Oceanography*, *22*(12), 1486–1505. https://doi.org/10.1175/1520-0485(1992)022<1486:SDTTIA>2.0.CO;2

Broxton, P. D., Zeng, X., & Dawson, N. (2017). The impact of a low bias in snow water equivalent initialization on CFS seasonal forecasts. *Journal of Climate*, *30*(21), 8657–8671. https://doi.org/10.1175/JCLI-D-17-0072.1

Cassou, C. (2008). Intraseasonal interaction between the Madden-Julian Oscillation and the North Atlantic Oscillation. *Nature*, *455*(7212), 523–527. https://doi.org/10.1038/nature07286

Cohen, J., Barlow, M., Kushner, P. J., & Saito, K. (2007). Stratosphere–troposphere coupling and links with eurasian land surface variability. *Journal of Climate*, *20*(21), 5335–5343. https://doi.org/10.1175/2007jcli1725.1

Cohen, J., Foster, J., Barlow, M., Saito, K., & Jones, J. (2010). Winter 2009–2010: A case study of an extreme arctic oscillation event. *Geophysical Research Letters*, *37*, L17707. https://doi.org/10.1029/2010GL044256

Cohen, J., Furtado, J. C., Jones, J., Barlow, M., Whittleston, D., & Entekhabi, D. (2014). Linking Siberian snow cover to precursors of stratospheric variability. *Journal of Climate*, *27*(14), 5422–5432. https://doi.org/10.1175/JCLI-D-13-00779.1

Counillon, F., Bethke, I., Keenlyside, N., Bentsen, M., Bertino, L., & Zheng, F. (2014). Seasonal-to-decadal predictions with the ensemble Kalman filter and the Norwegian Earth System Model: A twin experiment. *Tellus A*, *66*(1), 1–21. https://doi.org/10.3402/tellusa.v66.21074

Counillon, F., Keenlyside, N., Bethke, I., Wang, Y. G., Billeau, S., Shen, M.-L., & Bentsen, M. (2016). Flow-dependent assimilation of sea surface temperature in isopycnal coordinates with the Norwegian Climate Prediction Model. *Tellus A: Dynamic Meteorology and Oceanography*, *68*(1), 32,437. https://doi.org/10.3402/tellusa.v68.32437

Dee, D. P., Uppala, S. M., Simmons, A. J., Berrisford, P., Poli, P., Kobayashi, S., et al. (2011). The ERA-Interim reanalysis: Configuration and performance of the data assimilation system. *Quarterly Journal of the Royal Meteorological Society*, *137*(656), 553–597. https://doi.org/10.1002/qj.828

Dutra, E., Schär, C., Viterbo, P., & Miranda, P. M. (2011). Land-atmosphere coupling associated with snow cover. *Geophysical Research Letters*, *38*, L15707. https://doi.org/10.1029/2011GL048435

Evensen, G. (2003). The ensemble Kalman filter: Theoretical formulation and practical implementation. *Ocean Dynamics*, *53*(4), 343–367. https://doi.org/10.1007/s10236-003-0036-9

Fletcher, C. G., Hardiman, S. C., & Kushner, P. J. (2009). The dynamical response to snow cover perturbations in a large ensemble of atmospheric GCM integrations. *Journal of Climate*, *22*(5), 1208–1222. https://doi.org/10.1175/2008CLI2505

Furtado, J. C., Cohen, J. L., Butler, A. H., Riddle, E. E., & Kumar, A. (2015). Eurasian snow cover variability, winter climate, and stratosphere–troposphere coupling in the CMIP5 models. *Climate Dynamics*, *45*(9–10), 2591–2605. https://doi.org/10.1007/s00382-015-2494-4

Garfinkel, C. I., Son, S.-W., Song, K., Aquila, V., & Oman, L. D. (2017). Stratospheric variability contributed to and sustained the recent hiatus in Eurasian winter warming. *Geophysical Research Letters*, *44*, 374–382. https://doi.org/10.1002/2016GL072035

Halder, S., & Dirmeyer, P. A. (2016). Relation of Eurasian snow cover and Indian summer monsoon rainfall: Importance of the delayed hydrological effect. *Journal of Climate*, *30*(4), 1273–1289. https://doi.org/10.1175/JCLI-D-16-0033.1

Hardiman, S. C., Kushner, P., & Cohen, J. (2008). Investigating the ability of general circulation models to capture the effects of Eurasian snow cover on winter climate. *Journal of Geophysical Research*, *113*, D21123. https://doi.org/10.1029/2008JD010623

He, Q., Zuo, Z., Zhang, R., Yang, S., Wang, W., Zhang, R., & Riddle, E. E. (2016). Prediction skill and predictability of Eurasian snow cover fraction in the NCEP Climate Forecast System version 2 reforecasts. *International Journal of Climatology*, *36*(12), 4071–4084. https://doi.org/10.1002/joc.4618

Henderson, G. R., Peings, Y., Furtado, J. C., & Kushner, P. J. (2018). Snow–atmosphere coupling in the Northern Hemisphere. *Nature Climate Change*, *8*(11), 954–963. https://doi.org/10.1038/s41558-018-0295-6

Jeong, J. H., Lee, H., Yoo, J. H., Kwon, M. H., Yeh, S. W., Kug, J. S., et al. (2017). The status and prospect of seasonal climate prediction of climate over Korea and East Asia: A review. *Asia-Pacific Journal of Atmospheric Sciences*, *53*(1), 149–173. https://doi.org/10.1007/s13143-017-0008-5

Jeong, J. H., Linderholm, H. W., Woo, S.-H., Folland, C., Kim, B.-M., Kim, S.-J., & Chen, D. (2013). Impact of snow initialization on sub-seasonal forecasts of surface air temperature for the cold season. *Journal of Climate*, *26*(6), 1956–1972. https://doi.org/10.1175/JCLI-D-12-00159.1

Karspeck, A. R., Danabasoglu, G., Anderson, J., Karol, S., Collins, N., Vertenstein, M., et al. (2018). A global coupled ensemble data assimilation system using the Community Earth System Model and the Data Assimilation Research Testbed. *Quarterly Journal of the Royal Meteorological Society*, *144*(717), 2404–2430. https://doi.org/10.1002/qj.3308

Koster, R. D., Dirmeyer, P. A., Guo, Z., Bonan, G., Chan, E., Cox, P., et al., & GLACE Team (2004). Regions of strong coupling between soil moisture and precipitation. *Science*, *305*(5687), 1138–1140. https://doi.org/10.1126/science.1100217

Koster, R. D., Mahanama, S. P. P., Yamada, T. J., Balsamo, G., Berg, A. A., Boisserie, M., et al. (2010). Contribution of land surface initialization to subseasonal forecast skill: first results from a multi-model experiment. *Geophysical Research Letters*, *37*, L02402. https://doi.org/10.1029/2009GL041677

Koster, R. D., Mahanama, S. P. P., Yamada, T. J., Balsamo, G., Berg, A. A., Boisserie, M., et al. (2011). GLACE2: The second phase of the global land atmosphere coupling experiment: Soil moisture contribution to subseasonal forecast skill. *Journal of Hydrometeorology*, *12*(5), 805–822. https://doi.org/10.1175/2011JHM1365.1

Li, F., & Wang, H. J. (2014). Autumn Eurasian snow depth, autumn Arctic sea ice cover and East Asian winter monsoon. *International Journal of Climatology*, *34*(13), 3616–3625. https://doi.org/10.1002/joc.3936

Li, J. P., & Wang, J. X. L. (2003). A modified zonal index and its physical sense. *Geophysical Research Letters*, *30*(12), 1632. https://doi.org/10.1029/2003GL017441

Mariotti, A., Ruti, P. M., & Rixen, M. (2018). Progress in subseasonal to seasonal prediction through a joint weather and climate community effort. *npj Climate and Atmospheric Science*, *1*(1), 4. https://doi.org/10.1038/s41612-018-0014-z

Marsh, D. R., Mills, M. J., Kinnison, D. E., Lamarque, J. F., Calvo, N., & Polvani, L. M. (2013). Climate change from 1850 to 2005 simulated in CESM1 (WACCM). *Journal of Climate*, *26*(19), 7372–7391. https://doi.org/10.1175/JCLI-D-12-00558.1

Mudryk, L. R., Derksen, C., Kushner, P. J., & Brown, R. (2015). Characterization of Northern Hemisphere snow water equivalent datasets, 1981-2010. *Journal of Climate*, *28*(20), 8037–8051.

Oleson, K., Lawrence, D. M., Bonan, G. B., Drewniak, B., Huang, M., Koven, C. D., et al. (2013). Technical Description of version 4.5 of the Community Land Model (CLM), NCAR Technical Note NCAR/TN-503+STR, Boulder, Colorado, 420 pp.

Orsolini, Y. J., & Kvamstø, N. (2009). The role of the Eurasian snow cover upon the wintertime circulation: Decadal simulations forced with satellite observations. *Journal of Geophysical Research*, *114*, D19108. https://doi.org/10.1029/2009JD012253

Orsolini, Y. J., Senan, R., Balsamo, G., Doblas-Reyes, F., Vitart, D., Weisheimer, A., et al. (2013). Impact of snow initialization on sub-seasonal forecasts. *Climate Dynamics*, *41*(7–8), 1969–1982. https://doi.org/10.1007/s00382-013-1782-0

Orsolini, Y. J., Senan, R., Vitart, F., Weisheimer, A., Balsamo, G., & Doblas-Reyes, F. (2016). Influence of the Eurasian snow on the negative North Atlantic Oscillation in subseasonal forecasts of the cold winter 2009/10. *Climate Dynamics*, *47*(3-4), 1325–1334. https://doi.org/10.1007/s00382-015-2903-8

Peings, Y., Saint-Martin, D., & Douville, H. (2012). A numerical sensitivity study of the influence of Siberian snow on the northern annular mode. *Journal of Climate*, *25*(2), 592–607. https://doi.org/10.1175/JCLI-D-11-00038.1

Plumb, R. A. (1985). On the three-dimensional propagation of stationary waves. *Journal of the Atmospheric Sciences*, *42*(3), 217–229.

Smith, D. M., Scaife, A. A., Eade, R., & Knight, J. R. (2016). Seasonal to decadal prediction of the winter North Atlantic Oscillation: Emerging capability and future prospects. *Quarterly Journal of the Royal Meteorological Society*, *142*(695), 611–617. https://doi.org/10.1002/qj.2479

Sobolowski, S., Gong, G., & Ting, M. (2007). Northern Hemisphere winter climate variability: Response to North American snow cover anomalies and orography. *Geophysical Research Letters*, *34*, L16825. https://doi.org/10.1029/2007gl030573

Sospedra-Alfonso, R., Merryfield, W. J., & Kharin, V. V. (2016). Representation of snow in the Canadian seasonal to interannual prediction system. Part II: Potential predictability and hindcast skill. *Journal of Hydrometeorology*, *17*(5), 1467–1488. https://doi.org/10.1175/JHM-D-14-0223.1

Thomas, J. A., Berg, A. A., & Merryfield, W. J. (2016). Influence of snow and soil moisture initialization on sub-seasonal predictability and forecast skill in boreal spring. *Climate Dynamics*, *47*(1–2), 49–65. https://doi.org/10.1007/s00382-015-2821-9

van den Hurk, B., Doblas-Reyes, F., Balsamo, G., Koster, R. D., Seneviratne, S. I., & Camargo, H. (2012). Soil moisture effects on seasonal temperature and precipitation forecast scores in Europe. *Climate Dynamics*, *38*(1-2), 349–362. https://doi.org/10.1007/s00382-010-0956-2

Vitart, F., & Robertson, A. W. (2018). The sub-seasonal to seasonal prediction project (S2S) and the prediction of extreme events. *npj Climate and Atmospheric Science*, *1*(1), 3. https://doi.org/10.1038/s41612-018-0013-0

Vitart, F., Robertson, A. W., & Anderson, D. L. (2012). Subseasonal to seasonal prediction project: Bridging the gap between weather and climate. *Bulletin of the World Meteorological Organization*, *61*(2), 23.

Wang, Y. G., Counillon, F., Bethke, I., Keenlyside, N., Bocquet, M., & Shen, M.-L. (2017). Optimising assimilation of hydrographic profiles into isopycnal ocean models with ensemble data assimilation. *Ocean Modelling*, *114*, 33–44. https://doi.org/10.1016/j.ocemod.2017.04.007

White, C. J., Carlsen, H., Robertson, A. W., Klein, R. J. T., Lazo, J. K., Kumar, A., et al. (2017). Potential applications of subseasonal-to-seasonal (S2S) predictions. *Meteorological Applications*, *24*(3), 315–325. https://doi.org/10.1002/met.1654

Xu, L., & Dirmeyer, P. (2011). Snow-atmosphere coupling strength in a global atmospheric model. *Geophysical Research Letters*, *38*, L13401. https://doi.org/10.1029/2011GL048049

Xu, L., & Dirmeyer, P. (2013). Snow–atmosphere coupling Strength. Part I: Effect of model biases. *Journal of Hydrometeorology*, *14*(2), 389–403. https://doi.org/10.1175/JHM-D-11-0102.1